**Title** : Boundary Control with Corrected Second-order Switching Surface for Buck Converters Connected to Capacitive Loads

**Authors** :
† Isuru D.G. Jayawardana, *Student Member, IEEE*
† Carl N.M. Ho (Corresponding author), *Senior Member, IEEE*
* Yuanbin He

**Address** :
† University of Manitoba,
75 Chancellors Circle,
Winnipeg, MB, R3T 5V6,
Canada.
* College of Automation, Hangzhou Dianzi University,
Hangzhou 310000, China

**Tel.** :
† +1 204 474 7061
* +86 571 86915114

**Fax.** :
† +1 204 474 7522

**Email** :
† carl.ho@umanitoba.ca
† jayawari@myumanitoba.ca
* yuanbinhe@hdu.edu.cn

**Note** : This work was supported in part by a grant from the NSERC Discovery Grants program, Canada (Sponsor ID: RGPIN-2016-05952).

# Boundary Control with Corrected Second-order Switching Surface for Buck Converters Connected to Capacitive Loads

†Isuru D.G. Jayawardana, †Carl N. M. Ho and *Yuanbin He

*Abstract*- Boundary control with second-order switching surface is exploited for achieving faster response time and robust operation of switching power converters. However, the system performance of the boundary-controlled converters is significantly affected when it is connected to a second-stage converter with a large input capacitor. This paper studies the shortcomings in second-order boundary control schemes of buck converter with capacitive loads and non-linear switching loads. Secondly, the paper proposes a boundary control scheme with corrected second-order switching surface to drive buck converters cascaded to boost converters. The switching criteria of the corrected control law accounts for the effect of unknown load capacitance as well as the variation in filter parameters. Therefore, outer voltage ripple feedback loop is introduced to determine corresponding the switching criteria gain factor that adjusts the overall gain, while maintaining the output voltage ripple at a specified voltage band. The proposed method is verified by both simulation and hardware experiments. A 250 W buck converter prototype has been built to validate the control scheme under different load types including resistive-capacitive load, a boost converter and a commercial dc electronic load. A comparison is drawn between conventional boundary control and the proposed method in both simulation and experimental environment in order to highlight the advantages of the proposed method. With this approach, the converter operates at designed boundary control parameters independent of load capacitance and system parameter variations.

*Index Terms*— Boundary control, second-order switching surface, buck converter, cascaded buck-boost, capacitive load, non-linear load.

## I. INTRODUCTION

Digital boundary control methods are well established in modern switching power converters to achieve ultra-fast response time and robust operation compared to pulse-width modulated (PWM) control schemes. Boundary control (BC) is known as a geometric based control method that guides the state variables along a switching surface until it reaches the intended operating point [1]–[4]. Switching surface is defined as a boundary condition in the state plane that decides the state of the switches of the converter. The hysteresis control [5], [6] and sliding mode control(SMC) [7], [8] are the widely used BC methods with a first–order switching surface in which state variables are guided along a straight line. This results in multiple switching actions to reach the steady state during transients and leads for slower response time. The second-order sliding mode (SOSM) control methods are exploited using twist and optimal algorithms to achieve better transient responses compared to 1st order SMC method [9]–[11]. Moreover, by using BC with curved switching surfaces such as second-order switching surface ($\sigma^2$) [12]–[14], and natural switching surface(NSS) [15]–[17], the converter can achieve near optimal response for large signal disturbances.

In $\sigma^2$, a second-order switching surface is derived by predicting the trajectory of state variables of the converter after a switching action. Hence, $\sigma^2$ will enhance the tangential velocity of the trajectory along the switching surface which helps in providing a superior transient response over other boundary control methods with first order switching surface [13]. Further, it allows maintaining full control over the operation of a converter including start-up, transients and steady state conditions [12].Typically, $\sigma^2$ has been proposed for buck type converters [18]–[21] to regulate its output voltage by controlling the capacitor voltage at a specified voltage band ($\Delta$) which governs the switching frequency of the system. In [22], [23], boost-derived power factor correctors (PFCs) are proposed with $\sigma^2$ in the inner loop to control dc link voltage and it is shown that a steady state can be achieved within two switching actions. According to literatures, $\sigma^2$ provides a near-optimal switching surface while improving the system stability and system dynamic response. Despite its

advantages in settling time, dynamic response and system stability, $\sigma^2$ is sensitive to parameter variations [13]. Also, its performance is significantly affected when a second-stage converter is connected to it.

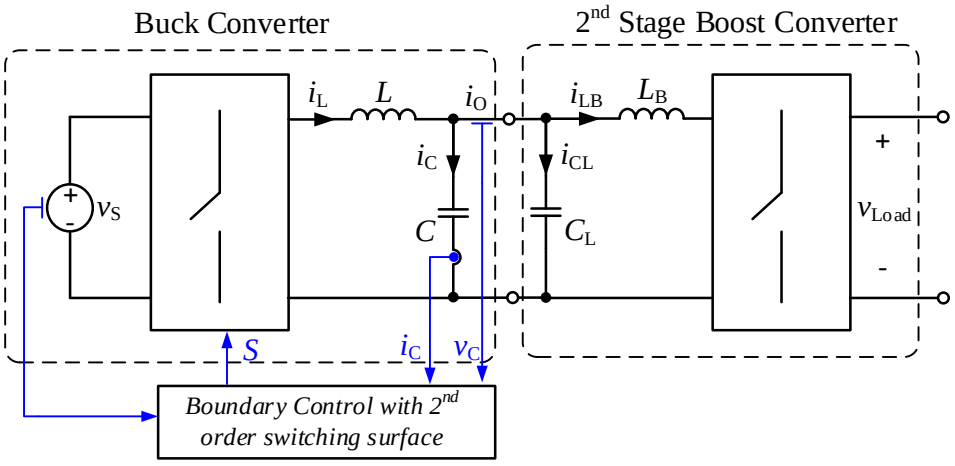


Fig. 1 General configuration of a system composed of buck converter cascaded to boost converter.

Fig. 1 shows the configuration of a cascaded system composed of a $\sigma^2$-controlled buck converter connected to a second stage boost converter. The second-stage converter mostly consists of a high frequency filtering input capacitor ($C_L$) that appears in parallel with the first-stage output filter capacitor ($C$). This parallel capacitor from the second-stage/load converter would result the change in original state-plane trajectories of the first-stage/source converter. As the switching surface of $\sigma^2$ relies on filter parameters, any change in these parameters would affect the state-plane trajectory that would directly lead to change in switching instances of the first-stage converter. Moreover, $\sigma^2$ depends on the instantaneous measurement of capacitor current and capacitor voltage, and its ripple may be affected by the ripple components generated by the switching actions of second-stage converter. Such discrepancies between the real system and designed switching criteria would lead to incorrect switching actions. This is a common problem in cascaded dc-dc converter systems where source converter control relies on capacitor current measurement, examples of such methods are SMC [7], natural switching surface [15] and $\sigma^2$ [12]. As a result, standard linear control methods such as

proportional–integral–derivative (PID) based on constant frequency PWM operation are widely adopted for control of first-stage buck converters [24]. In cascaded dc-dc configuration, careful attention is required for the design of such controller which is done generally by analysing the stability of the minor loop gain of the cascaded system [25]. Further, linear control method has a shortcoming in achieving faster response for applications that demands it. Different large-signal based control approaches like proximate time-optimal control [26], [27] and SOSM [9], that uses capacitor current estimator are presented to improve transient response and robustness of buck converters. Nevertheless, the $\sigma^2$ method is a promising option to achieve fast dynamic performance for buck converter with linear loads given the fact it can reach steady state within two switching actions. The performance of $\sigma^2$ in a cascaded configuration with a load converter has not been investigated in detail in the literature. Applying conventional $\sigma^2$ for a cascaded configuration, would yield incorrect switching actions and specified control parameters cannot not be maintained. It is, therefore, desirable to correct the boundary control law by considering the impact from second-stage converter, while preserving fast response characteristics.

This study aims to extend the conventional $\sigma^2$ method to control a buck converter cascaded to a boost converter (hereafter referred as cascaded buck-boost) as shown in Fig 1. The second-stage boost converter is considered to represent capacitive loads. The cascaded dc-dc configuration shown in Fig. 1 is a typical configuration for a system that uses a buck stage as a source converter and can be seen in applications such as non-isolated switch-mode power supply [28], photovoltaic (PV) emulator [29], [30] and fuel cell emulator [31]. In source emulators, buck converter is mostly used as the controlled power source to emulate the required source model and second-stage boost converter is connected as the device under test. Both dc power supplies and source emulators demand a faster transient response to emulate true source characteristics [32]. Targeting such applications, this paper presents a boundary control scheme with corrected switching surface ($\sigma_{cor}^2$) for buck converters connected to second-stage boost converters. The proposed switching surface is derived by considering the presence of load

capacitance as well as addressing any switching criteria gain mismatches due to filter parameter variations. Further, it is derived considering the fact that the switching ripple components of the buck-stage is not visible in the boost-stage inductor due to high frequency filtering capacitors $C$ & $C_L$ and also, under the condition that the magnitude of current ripple components passing through $C$ and $L$ due to switching of second-stage boost converter is negligible compared to the magnitude of first-stage current ripple components, $i_C$ and $i_L$. This is a valid condition for cascaded buck-boost configuration since boost-stage inductor is typically designed to maintain its current ripple to be around ~20% of the nominal value and large $C_L$ is placed to filter high frequency signal of the input current of the converter [33]–[35]. The outer voltage ripple feedback loop is introduced to determine a corresponding switching criterion gain factor that accounts for mismatch due to additional load capacitance as well as any variations in filter parameters in the real system.

This paper is organized as follows; Section II discusses the basic principle of $\sigma^2$ for buck dc–dc converters and its limitations in general as well as in cascaded buck-boost configurations. The detailed derivation of the $\sigma_{cor}^2$, design procedures of outer loop control as well as voltage ripple measurement method are presented in Section III. The performance of proposed method is verified with simulation and experimental results of a 250 W 120V/50V buck converter prototype and results are presented in Section IV and Section V respectively.

## II. Overview of $\sigma^2$ with Buck Converters

The basic principle of $\sigma^2$ builds on state trajectories of the buck converter and guiding the converter in near optimal manner to achieve control objectives. Switching criteria are determined by identifying the right moment to turn ON or OFF as movement of voltage and current can be predicted based on steady state operation of the converter. The switching criteria considers the area under capacitor current ($i_C$) with a hypothesized switching action until $i_C = 0$, and comparing this area with a fixed ratio of the output voltage error instantaneously [12]. This assumes that output current

($i_O$) is relatively constant by considering the load as pure resistive ($R_L$) and change of $i_L$, $\Delta i_L$ equals to the change of $i_C$, $\Delta i_C$. Fig. 2 shows the buck converter schematics with a resistive load. The switching criteria for buck converter can be derived as below

$$v_{C,min} \leq v_C - k_1 {i_C}^2 \quad , i_C < 0 \tag{1}$$

$$v_{C,max} \geq v_C + k_2 {i_C}^2 \quad , \; i_C > 0 \tag{2}$$

where $v_{C,min} = v_{ref} - \Delta$, $v_{C,max} = v_{ref} + \Delta$ and $k_1$, $k_2$ are constants. The ideal values of $k_1$ and $k_2$ are;

$$\{k_1, k_2\} = \left\{ \frac{L}{2\,C(V_S - V_{ref})}, \frac{L}{2\,C\,V_{ref}} \right\} \tag{3}$$

A detailed derivation of (1)-(3) can be found in [13]. The critical parameters of the system are tabulated in Table I. $k_1$ and $k_2$ are calculated using nominal values of $L$ and $C$. Fig. 3 shows the switching trajectory of $\sigma^2$ from starting up to target operating point on the $v_C - i_L$ state plane for a resistive load. This illustrates that system reaches steady-state within two switching actions while maintaining the defined voltage band. Ideal state on and off trajectories are obtained by solving state-space equations of the converter for different initial conditions. The on-state trajectories are represented in solid lines and off-state trajectories are represented in dotted lines.

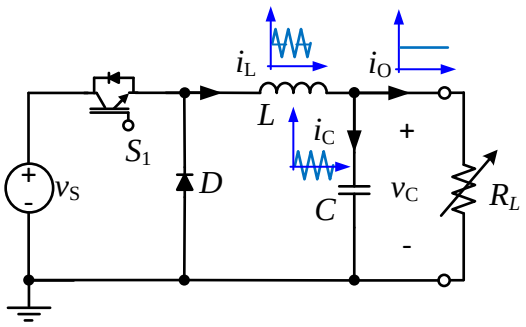


Fig. 2 Circuit schematics of buck converter with a resistive load.

TABLE I
PARAMETER VALUES OF BUCK CONVERTER

| Parameter | Value | Parameter | Value |
|---|---|---|---|
| $v_s$ | 120 V | $L$ | 3.5 mH |
| $v_{ref}/\Delta$ | 50 V/2V | $C$ | 4.7 µF |

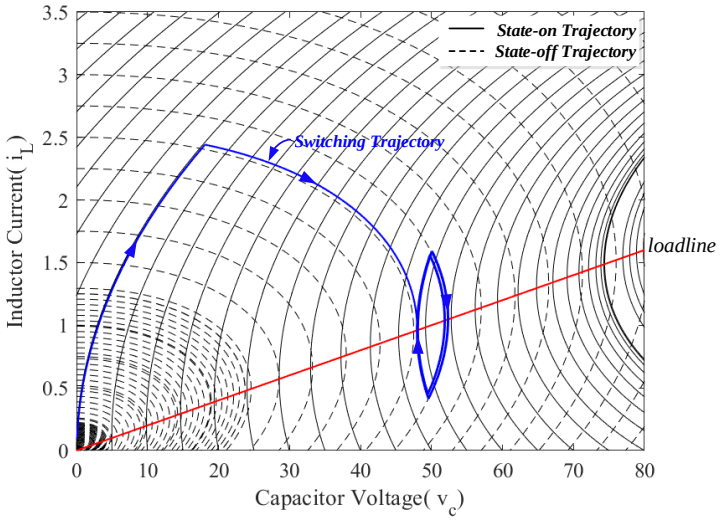


Fig. 3 System trajectories on the inherent state plane with σ^2 for a resistive load from start up to steady-state operation.

### *A. Limitations with conventional $\sigma^2$*

The switching criteria of $\sigma^2$ is a function of parameters such as $L$ and $C$. Hence, if practical $L$ and $C$ values in the converter are different from the nominal values considered in the switching criteria, $\sigma^2$ leads the converter to operate with inaccurate voltage ripple, switching frequency and average output voltage [13]. In the worst case, deviation in voltage ripple may even cause the converter to operate in discontinuous conduction mode (DCM). These deviations will be aggravated when $\sigma^2$ controlled buck converter is cascaded to a non-linear switching converter for the reasons of having a large input capacitance and also, due to current ripple components brought in by the second-stage converter. In cascaded configurations, current ripple components led by both first and second-stage converters would pass through $C$ and $C_L$.Thus, the shape of $i_C$ waveform cannot be approximated as a triangular in steady state and the steps taken to derive conventional $\sigma^2$ in [12] would no longer be valid. The second-stage converter commonly consists of input capacitor ($C_L$) to filter high frequency ripple components in the input current [35]. Existence of $C_L$ would change the

equivalent capacitance seen by the first stage converter, to $C + C_L$ as $C_L$ will be directly connected in parallel with $C$. Inductor current ripple is shared between $C$, $C_L$ and input branch of the second-stage converter based on their impedance. Hence, the assumption that is taken in [12] to derive the switching criteria of $\Delta i_L$ equals to $\Delta i_C$ is violated. Also, capacitance considered in the switching criteria is different from the real circuit. These scenarios create a discrepancy between the system used to derive the switching criteria and the real system. **Error! Reference source not found.** shows the movement of converter on the $v_C - i_L$ state plane, when the buck converter is connected to a resistive-capacitive load. This shows that the converter operates with larger voltage and current ripple as a result of incorrect switching actions. Even though $\sigma^2$ has above mentioned limitations, it features with much superior dynamic response characteristics and robust operation over wide range of the converter. Hence it is necessary to overcome issues related to connecting to capacitive loads as well as non-linear switching loads.

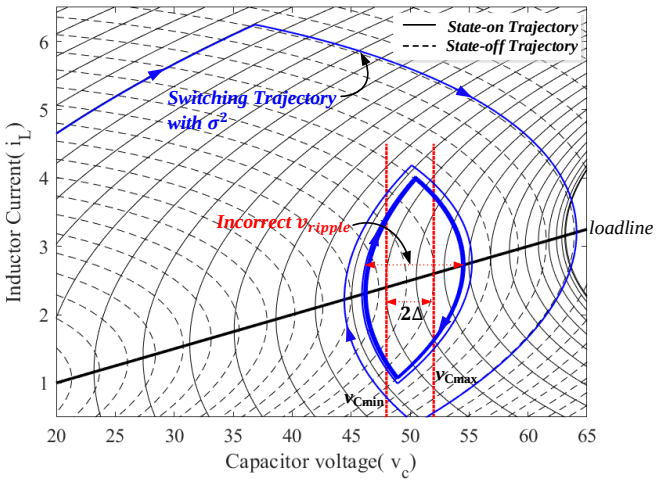


Fig. 4 $\sigma^2$ switching trajectories on the inherent state plane with Resistive-capacitive load ( $R_L$=20 Ω, $C_L$=10 µF, $v_{ref}$=50 V and $\Delta$ =2 V).

In cascaded buck-boost configuration, the boost-stage inductor acts as a low conductance path for high frequency current ripple components of the buck-stage inductor current and vice versa. The parallel capacitors are typically designed to have a significantly high conductance path for current ripple components of $i_L$. Hence the current ripple components of $i_L$ passing through $L_B$ is

negligible. Similarly, it can be understood that the current ripple components of boost stage inductor current ($i_{LB}$) is not visible in $i_L$. i.e., if the impedance of each inductor at high frequencies (in the range of switching frequency) is 30 times higher than impedance of the combined capacitor branches, only 3.3% of current ripple components are passing through the opposite stage inductor. Thus, it can be concluded that current ripple of $i_L$ will be shared mainly with capacitor branches ($C$ and $C_L$) and it will be free from current ripple component led by boost stage. **Error! Reference source not found.** shows how current ripple components would interact among passive elements in the cascaded buck-boost configuration. Further, under conditions of current ripple of $i_{LB}$ is maintained smaller than the current ripple of $i_L$ and $C_L$ is much larger than $C$, it can be approximated that current ripple component passing through $C$ due to the switching of boost converter is negligible. These are valid conditions for a boost converter since the current ripple of the boost inductor is designed to maintain around ~20% of the nominal value and large $C_L$ is placed to filter high frequency signal of the input current [33]–[35]. Based on above considerations, derivation of a corrected boundary control with second-order switching surface ($\sigma_{cor}^2$) is presented in the next section.

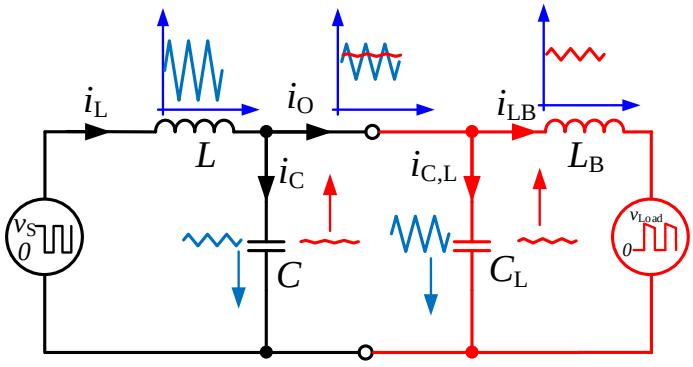


Fig. 5 Simplified equivalent circuit of the cascaded buck-boost system.

## III. Control Law Formulation

Fig. 1 shows the system structure that consists of a boundary-controlled buck converter cascaded to a boost converter. The boost converter consists of an input capacitive-inductive filter. Fig. 6 shows the architecture of the complete system which consists of four main elements, including

the power conversion stage (PCS), boundary controller with corrected second-order switching surface ($\sigma_{cor}^2$), voltage ripple measurement block and the error amplifier (EA). Firstly, voltage ripple measurement block identifies the peak to peak ripple of $v_C$ ($\Delta_m$) using $i_L$ and $v_C$. Then, $\Delta_m$ is compared with a reference voltage band ($\Delta$) using EA. The output of the error amplifier, $k_D$ is used to adjust the deviation of switching criteria gains of $\sigma_{cor}^2$ due to filter parameter variations. The $\sigma_{cor}^2$ determines switching instants for $S_1$ in PCS based on $v_C$, $i_C$, $v_S$, $v_{ref}$, $\Delta$ and $k_D$.Thus, above mentioned elements forms a controller scheme to regulate $v_C$ together with a feedback loop for regulating $\Delta_m$ with considering effect of $C_L$.

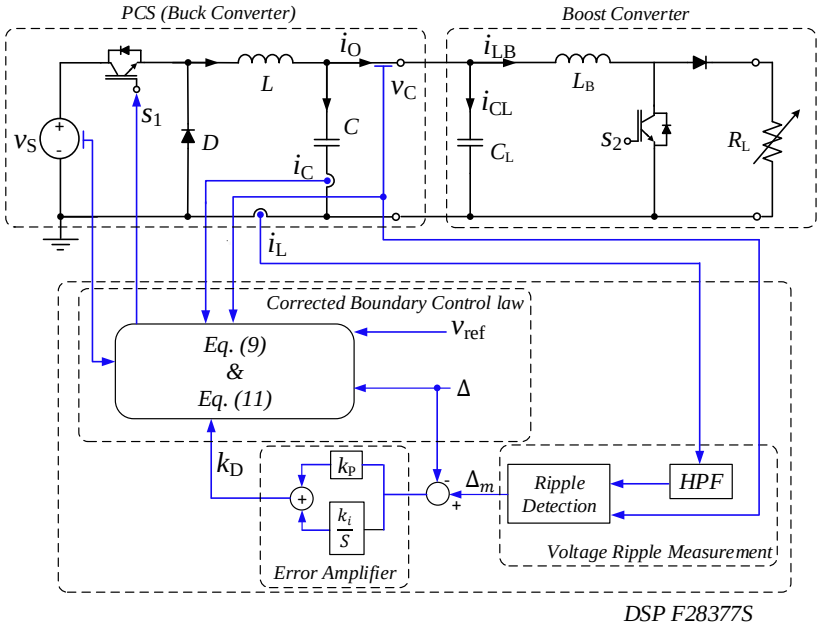


Fig. 6 Architecture of the corrected boundary control scheme.

### A. *Derivation of* $\sigma_{cor}^2$

The PCS operates with two states, namely Turn-ON state and Turn-OFF state in one switching cycle. The key time-domain waveforms of the system are shown in Fig. 7. Following derivations are done assuming all components are ideal. Based on the capacitor voltage equations at common output node for both $C$ and $C_L$, the relationship between slope of $i_C$ and slope of $i_{CL}$ is derived as,

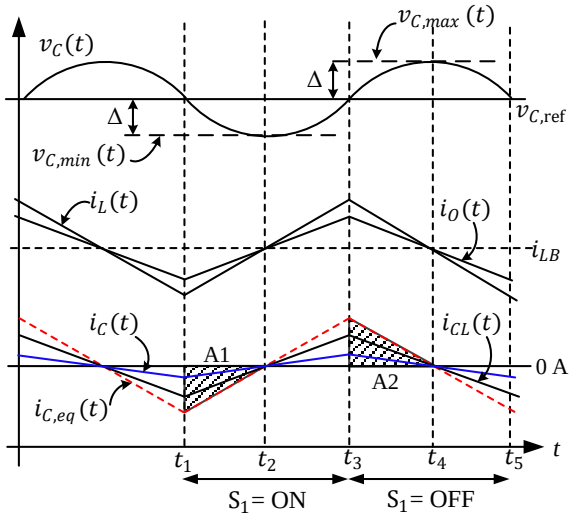


Fig. 7 Typical waveforms of $v_C$, $i_L$, $i_O$ and $i_C$.

$$\frac{di_{CL}(t)}{dt} = \frac{C_L}{C}\frac{di_C(t)}{dt} \tag{4}$$

Applying Kirchhoff's current law at the output node,

$$i_C(t) = i_L(t) - i_O(t) \tag{5}$$

where $i_O = i_{CL} + i_{LB}$, and as explained before, $i_{LB}$ is constant dc current from the buck converter perspective and it is free from ripple. With this assumption, (5) can be differentiated to estimate the slope of $i_C$ as;

$$\frac{di_C(t)}{dt} \cong \frac{di_L(t)}{dt} - \frac{di_{CL}(t)}{dt} \tag{6}$$

Thus, combining (4) and (6),

$$\frac{di_L(t)}{dt} \cong (1 + k_D)\frac{di_C(t)}{dt} \tag{7}$$

where $k_D = \frac{C_L}{C}$.

Further, following the similar method described in [12], boundary control law can be formulated by incorporating $k_D$. This $k_D$ represents the adjustments in switching criteria gains $\{k_1, k_2\}$ due to the appearance of $C_L$. The corrected boundary law is derived considering the steady state characteristics during Turn-ON state and Turn-OFF state of the buck converter.

*Switch ON Criteria*

Switching ON criteria is derived by determining $t_1$ such that $v_C$ will reach the lower boundary $v_{C,min}$ at $t_2$ at which $i_C = 0$. Assumed that $i_C$ varies linearly in Turn-ON state. Thus, during $t_1$-$t_2$ capacitor voltage is expressed by;

$$v_{C,min} = -\left[\frac{L}{2C}\frac{1}{v_S - v_{ref}}\right][1 + k_D]{i_C}^2(t_1) + v_C(t_1) \tag{8}$$

Detailed derivation of (8) is given in Appendix. In order to ensure that $v_C$(t) would not reach below $v_{Cmin}$, switching ON criteria for $S_1$ is derived using (8),

$$v_{C,min} \leq -\left[\frac{L}{2C}\frac{1}{v_S - v_{ref}}\right][1 + k_D]{i_C}^2 + v_C \;\&\; i_C < 0 \tag{9}$$

*Switch OFF Criteria*

The objective is to determine a time instant $t_3$ such that $v_C$ will reach the upper boundary $v_{C,max}$ at $t_4$ at which $i_C = 0$. Thus, during $t_3$-$t_4$ capacitor voltage is expressed by;

$$v_{C,max} = \left[\frac{L}{2C_{eq}}\frac{1}{v_{ref}}\right][1 + k_D]{i_C}^2(t_3) + v_C(t_3) \tag{10}$$

Detailed derivation of (10) is given in Appendix. In order to ensure that $v_C$(t) would not reach beyond $v_{Cmax}$, switching OFF criteria for $S_1$ is derived as,

$$v_{C,max} \geq \left[\frac{L}{2C}\frac{1}{v_{ref}}\right][1 + k_D]{i_C}^2 + v_C \;\&\; i_C > 0 \tag{11}$$

Based on (11) and (13), switching surface of $\sigma^2_{cor}$ can be concluded as,

$$\sigma^2_{cor,\Delta-} = \{(v_C - v_{min} - k'_1(i_C)^2, i_C < 0\} \tag{12}$$

$$\sigma^2_{cor,\Delta+} = \{(v_C - v_{max}) + k'_2(i_C)^2, i_C > 0\} \tag{13}$$

where $k'_1$ and $k'_2$ are constants.

$$\{k'_1, k'_2\} = \{k_1[1 + k_D], k_2[1 + k_D]\} \tag{14}$$

The $\sigma_{cor}^2$ requires instantaneous values of $v_C, i_C$ and $k_D$ to determine the switching actions. The values of $k_1$ and $k_2$ are constants and defined with nominal parameters as given in Table 1.

*B. Output Voltage Ripple Amplitude Detection*

The output voltage ripple amplitude ($\Delta_m$) is used as the feedback variable in the outer control loop. Determining the peak-peak ripple of $v_C$ over a switching cycle may not be straightforward since $v_C$ is mixed with voltage ripple components introduced by the second-stage converter. In contrast, the inductor current ($i_L$) is unaffected by the current ripple components led by the switching of second-stage converter as they are filtered out by $C$ and $C_L$. The $i_L$ waveform is, therefore, much smoother than $v_C$ as it only consists of current ripple components produced by the first-stage. Hence, $\Delta_m$ is determined considering the instantaneous values of both $i_L$ and $v_C$. Algorithm of the voltage ripple measurement block implemented in a software platform is shown in Fig. 8. Measured $i_L$ is passed through a high pass filter (HPF) to eliminate the dc offset and obtain the ac signal of $i_L$ ($i_{LH}$). Cut-off frequency of the HPF is designed to be lower than the minimum switching frequency of the system.

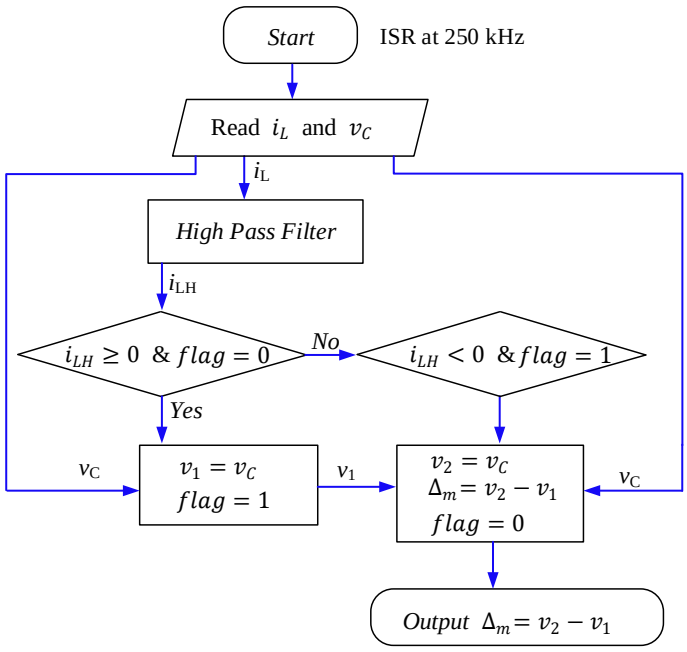


Fig. 8 Flow chart for $\Delta_m$ measurement.

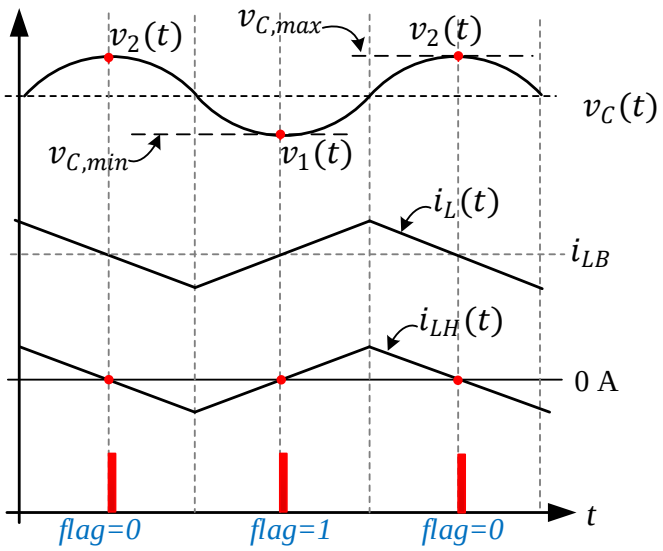


Fig. 9 Key waveforms of voltage ripple amplitude detection.

Fig. 9 shows that $v_C$ would be at a minimum, $v_{C,min}$ when $i_{LH}$ is crossing zero from negative side and $v_C$ would be at a maximum, $v_{C,max}$ when $i_{LH}$ is crossing zero from positive side. Hence, at the zero crossings of $i_{LH}$, a flag is triggered to store the instantaneous values of $v_C$. Then voltage ripple magnitude is calculated at each switching cycle based on stored values.

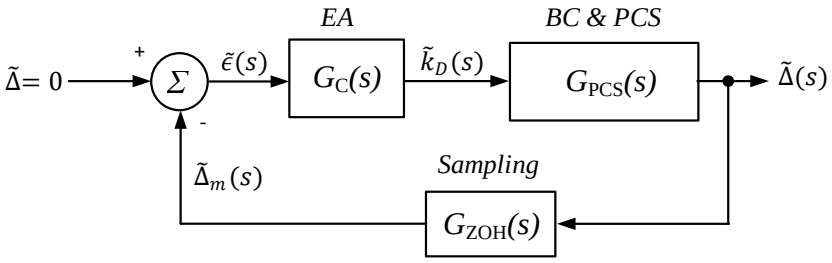


Fig. 10 Small signal control block diagram for the outer feedback loop.

### *C. Design of Outer Feedback Control Loop*

The value of $k_D$ is dependent on $C_L$ which is typically unknown as the second-stage boost converter is often a black-box. Hence, outer control loop is employed to determines the $k_D$ using an output voltage ripple feedback loop. Small signal analysis with bode plots is considered to study and design the EA parameters of the outer loop. Fig. 10 shows the small signal control block diagram of

the outer voltage ripple feedback loop. The measured $v_C$ ripple magnitude ($\Delta_m$) is compared with specified voltage ripple ($\Delta$) to check whether boundary controller maintains it to the specified value. The voltage ripple error is amplified by EA to generate the required $k_D$ based on the feedback loop mechanism shown in Fig. 10. The small signal $k_D$-to-voltage ripple transfer function (TF) is derived based on the large-signal large signal relationship between $\Delta$ and $k_D$. In [19], a large-signal relationship between switching frequency ($f_S$) and $\Delta$ of a $\sigma^2$-controlled buck converter is derived in detail . Following a similar procedure, large-signal relationship between $\Delta$ and $k_D$ is derived using state equations during Turn-ON state and Turn-ON state as well as considering the $\sigma_{cor}^2$ switching criteria equations. Switching frequency of the systems is given as,

$$f_S = HK\Delta^{-0.5}(1 + k_D)^{-0.5} \tag{15}$$

where $H = \frac{v_{ref}(v_S - v_{ref})}{Lv_S}$ and $K = \frac{\sqrt{k_1 k_2}}{\sqrt{2dk_1} + \sqrt{2(1-d)k_2}}$.

A detailed derivation of (15) is given in Appendix. Further, (15) can be simplified to determine the relationship between $k_D$ and $\Delta$.

$$k_D^{0.5} = \left(\frac{HK}{f_S}\right)\Delta^{-0.5} - 1 \tag{16}$$

Linearizing (16) at a steady operating point would yield the small signal TF between $\Delta$, and $k_D$.

$$G_{PCS}(s) = \frac{\tilde{\Delta}(s)}{\tilde{k}_D(s)} = -\left(\frac{HK}{f_S}\right)\bar{k}_D^{-0.5}\bar{\Delta}^{-1.5} \tag{17}$$

Further, transfer function of the inner boundary control loop is assumed to be constant since crossover frequency of outer voltage ripple feedback loop will be designed much lower than switching frequency. Hence, the $\tilde{k}_D(s)$ -to- $\tilde{\Delta}$ TF of $G_{PCS}(s)$ including inner $\sigma_{cor}^2$ -controlled loop is represented by (17).The ripple measurement block is modelled as a continuous zero order hold (ZOH) to represent discretization process and the time delays. As shown in Fig. 8 , the $\Delta_m$ is calculated in every half switching cycle, the transfer function of ZOH can be written as,

$$G_{ZOH}(s) = \frac{1-e^{-\frac{sT_S}{2}}}{\frac{sT_S}{2}} \quad (18)$$

where $T_S = \frac{1}{f_S}$ is the switching time period of the system. The EA is implemented using a Proportional-Integral (PI) controller and transfer function, $G_C(s)$ is given below in (19).

$$G_C(s) = -(K_P + \frac{K_i}{s}) \quad (19)$$

Since the gain of $G_{PCS}(s)$ is negative, the PI controller is designed with negative parameters to introduce a positive loop gain to the system. Thus, compensated open-loop gain $T_{OL}(s)$ of the outer voltage ripple feedback loop is expressed as,

$$T_{OL}(s) = G_{PCS}(s)G_{ZOH}(s)G_C(s) \quad (20)$$

By calculating the uncompensated open-loop TF (i.e. $T_{OLuc}(s) = G_{PCS}(s)G_{ZOH}(s)$), the $G_C(s)$ can be designed with frequency response methods. Fig. 11 shows bode plot of $T_{OLuc}(s)$ for different switching frequencies that is calculated based on parameters given in Table II. The EA is designed in such way that the crossover frequency of open loop transfer function of outer loop is at least 10 times lower than the minimum switching frequency present in the system. The uncompensated plant of the outer feedback loop is a non-minimum phase system with the characteristics of $G_{zoh}(s)$. The transfer function of $G_{zoh}(s)$ depends on the switching frequency of the converter. Hence, crossover frequency of the outer loop should be designed much lower than minimum expected frequency. Further, this will decouple inner boundary control dynamics from the outer feedback control loop. The minimum $f_S$ of the buck converter prototype in Section V is considered as 1.12 kHz that is calculated based on the parameters given Table II. Considering these guidelines and minimum $f_S$, EA is designed with $K_P$ =0.2 and $K_i$=400 to obtain a crossover frequency of 33 Hz as shown in Fig 11.

The bandwidth of outer feedback loop decides the response time of the $k_D$ that compensates the output voltage ripple. Here, $k_D$ is an additional gain factor which determines the correct switching surface. Hence, outer loop does not decrease the transient response time of the inner boundary controller. The outer loop bandwidth only has an effect during start-up transients since $C_L$ is changed only when new capacitive load is connected. However, system still reaches target operating point with two switching actions and specified output voltage ripple is achieved based on the outer loop bandwidth. The validity of above statements is confirmed by the experimental measurements in Section V.

TABLE II
PARAMETER VALUES USED IN SIMULATIONS

| $f_S$ = 8.42 kHz | | $f_S$ = 3.25 kHz | | $f_S$ = 1.12 kHz | |
|---|---|---|---|---|---|
| Parameter | Parameter | Parameter | Value | Parameter | Value |
| $v_S/v_{ref}$ | 120 V/ 50V | $v_S/v_{ref}$ | 120 V/ 50V | $v_S/v_{ref}$ | 120 V/ 50V |
| $L$ | 3.5 mH | $L$ | 3.5 mH | $L$ | 3.5 mH |
| $C$ | 4.7 µF | $C$ | 4.7 µF | $C$ | 4.7 µF |
| Δ | 0.5 V | Δ | 2 V | Δ | 2 V |
| $C_L$ | 10 µF | $C_L$ | 20 µF | $C_L$ | 200 µF |

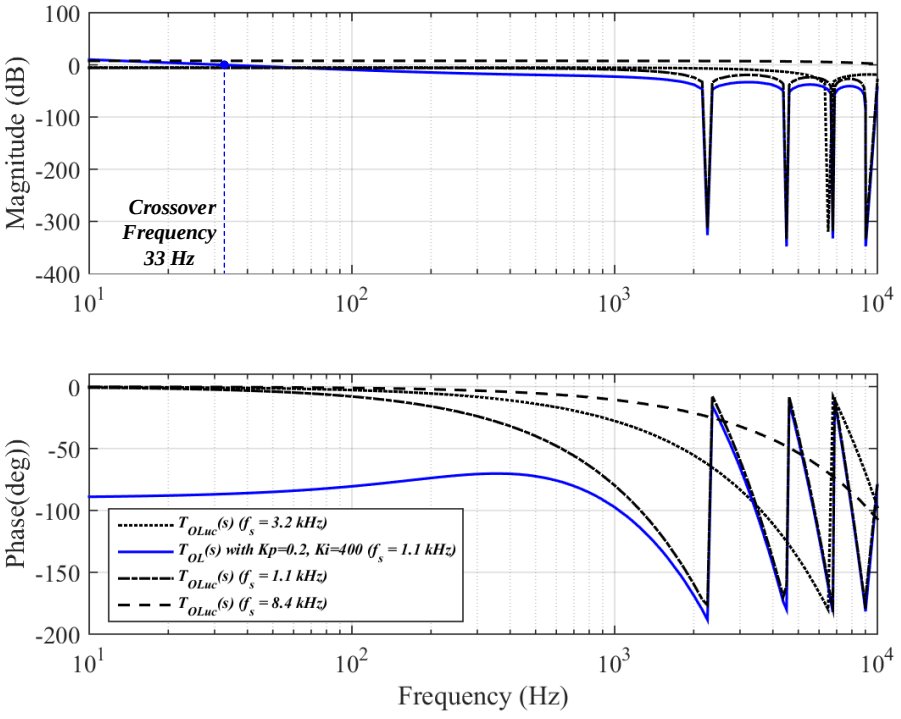


Fig. 11 Frequency response of the loop gain with different switching frequencies.

*D. Average Output Voltage and Output Voltage Ripple*

The expressions for average output voltage ($v_{C,Avg}$) and output voltage ripple ($v_{ripple}$) are derived based on the steady-state trajectories with $\sigma_{cor}^2$.

$$v_{C,Avg} = v_{ref} + \frac{\left(\frac{L}{2\,C\,v_{ref}} - \frac{L}{2\,C\,(v_S - v_{ref})}\right)\frac{1}{1+k_D} - (k_2' - k_1')}{k_1' + k_2'}.\Delta \tag{21}$$

$$v_{ripple} = v_{Cmax} - v_{Cmin} = \frac{L\Delta}{C(1+k_D)(k_1'+k_2')}\frac{v_S}{v_{ref}(v_S - v_{ref})} \tag{22}$$

A detailed derivation of average output voltage and output voltage ripple expressions with conventional $\sigma^2$ can be found in [13]. A similar approach is used to derive (21) and (22). If $k_1'$ and $k_2'$ are ideal values, (21) and (22) can be simplified to;

$$v_{C,Avg} = v_{ref} \tag{23}$$

$$v_{ripple} = 2\Delta \tag{24}$$

*E. Effect of Variation in Filter Parameters*

The corrected switching laws represented in (9) and (11) are derived considering the addition of $C_L$ and it has not addressed the deviation in filter parameters. If deviations are considered in $L$ and $C$, they can be expressed as,

$$L' = L(1+\alpha) \tag{25}$$

$$C' = C(1+\beta) \tag{26}$$

where α and β are the tolerances of $L$ and $C$ respectively. Substituting $L$ and $C$ values in (9) and (11) by $L'$ and $C'$ in (25) and (26) respectively. The switching ON and OFF criteria of $\sigma_{cor}^2$ with filter parameter variations can be expressed as,

$$v_{C,min} \leq -\left[\left[\frac{L}{2C}\frac{1}{v_S - v_{ref}}\right]k_D'\right]{i_C}^2 + v_C \;\&\; i_C < 0 \tag{27}$$

$$v_{C,max} \geq \left[\left[\frac{L}{2C}\frac{1}{v_{ref}}\right] k_D'\right] {i_C}^2 + v_C \;\&\; i_C > 0 \qquad (28)$$

where $k_D^{'} = \frac{(1+k_D)(1+\alpha)}{(1+\beta)}$.

The above switching criteria derived is in similar form as the original criteria in (9) and (11); the only difference being the gain $k_D^{'}$ which contains the original gain $k_D$ along with the factor of filter parameter variations. The outer voltage ripple feedback loop is still capable of determining the new switching gain factor, $k_D'$ which is directly corresponding to $C_L$, $\alpha$ and $\beta$ of the real system.

## IV. Simulation Results

Simulations are carried out to validate the proposed $\sigma_{cor}^2$ for a cascaded buck-boost system with (a) boost converter with open loop control and (b) boost converter as a constant power load. The system parameters used in the simulation is listed in Table III.

### *A. Boost converter with open loop control*

Fig. 12 illustrates the steady-state converter trajectory on $i_L$-$v_C$ state plane with the proposed $\sigma_{cor}^2$ and $\sigma^2$, when boost converter is acting as a load and it is operated with open loop control. The converter trajectory with both $\sigma_{cor}^2$ and $\sigma^2$ closely follows the state on and off trajectories, which are drawn considering both $C$ and $C_L$. The proposed $\sigma_{cor}^2$ regulates the output voltage at specified voltage band, whereas with $\sigma^2$, there is a significant error in output voltage ripple and runs into DCM.

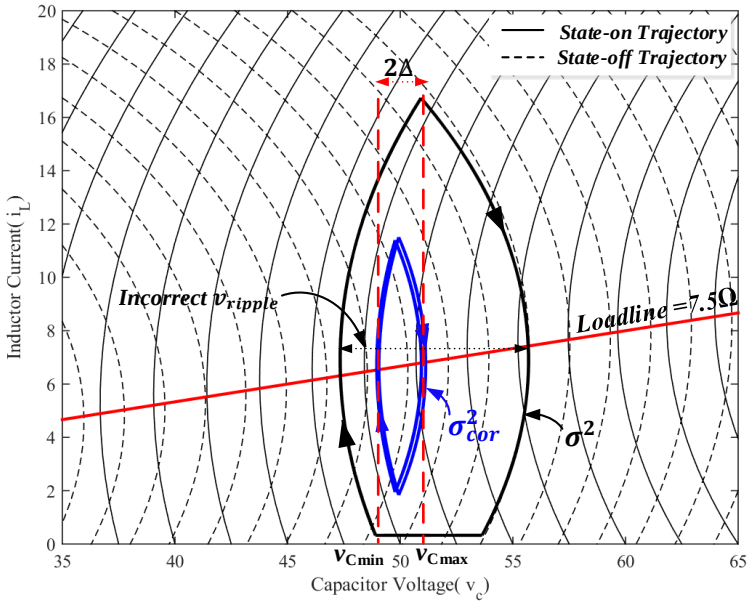


Fig. 12 Steady-state system trajectories for $\sigma^2$ and $\sigma^2_{cor}$ when boost converter with open loop control ($R_L$=50Ω).

Transient performance for proposed and conventional boundary controller is shown in Fig. 13 by changing the resistive load of the boost converter from 15 Ω to 7.5 Ω. Under the $\sigma^2_{cor}$, voltage band is accurately maintained at specified value as expected and operating $f_S$ is at 30.3 kHz. While with $\sigma^2$, there is a significant error in the voltage ripple due to inaccurate switching actions. The transient behavior of output voltage and current under both control schemes is similar. It can be observed that output current response is slower and takes ~1.8ms to reach steady state condition. Since the boost converter is operated with open loop control, the transient response depends on the cut-off frequency of the low pass filter (LPF) formed by $C, C_L$ and $L_B$.

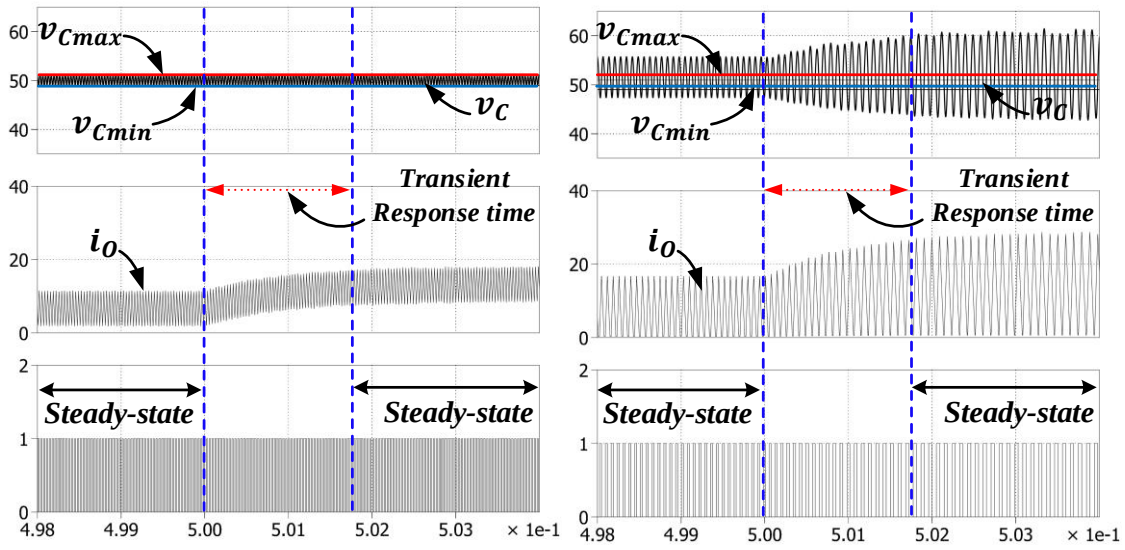


(a) (b)

Fig. 13 Time domain output waveforms for a boost-stage load transient (15 Ω to 7.5 Ω) (a) with $\sigma_{cor}^2$ (b) with $\sigma^2$.

### *B. Boost converter as a constant power load*

In case of constant power load, input current of the boost converter must be regulated and its dynamic response will be relying on the control bandwidth of the boost-stage current controller.

Fig. 14 (a) and (b) show the output waveforms of buck converter with $\sigma_{cor}^2$ when boost converter is regulated with a control bandwidth of ~700 Hz and 7 kHz respectively. The response of the output voltage ($v_C$) after a load transient, is much faster due to boundary control and it reaches steady state within one or two switching actions while maintaining the voltage ripple at specified value. As expected, the output current transient is much faster with higher control bandwidth system. Results shows a good agreement with the theory.

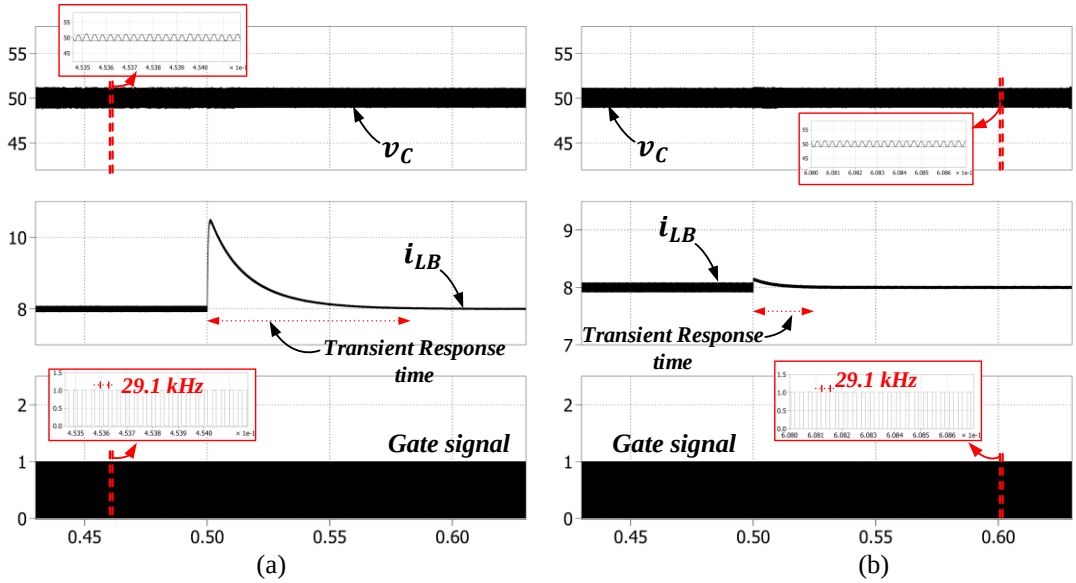


Fig. 14 Time domain output waveforms for a load transient when boost converter is regulated as constant power load (15 Ω to 7.5 Ω) (a) for a control bandwidth of 700 Hz (b) for a control bandwidth of 7 kHz.

TABLE III
PARAMETER VALUES USED IN SIMULATIONS

| BUCK STAGE | | BOOST STAGE | |
|---|---|---|---|
| Parameter | Value | Parameter | Value |
| $v_S$ | 120 V | $L_B$ | 3.5 mH |
| $v_{ref}$ | 50 V | $C_L$ | 20 µF |
| $L$ | 0.1 mH | $f_{S2}$ | 50 kHz |
| $C$ | 1 µF | $d_{openloop}$ | 0.5 |
| Δ | 1V | | |

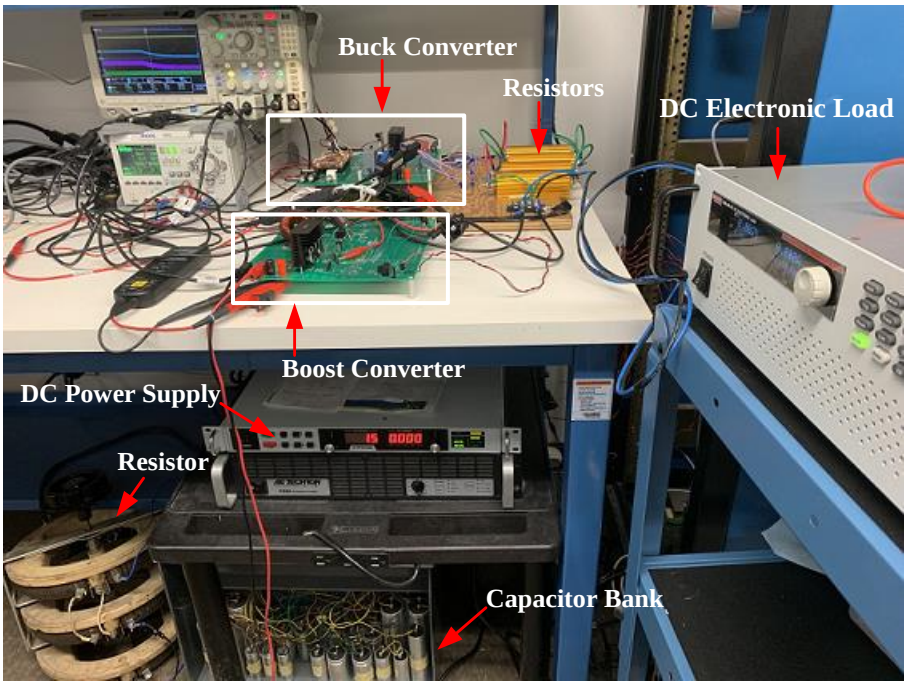


Fig. 15 Experimental test setup.

## IV. EXPERIMENTAL VALIDATION

In this section, proposed control scheme is verified with a 250 W buck converter prototype and experimental test setup is shown in Fig. 15. The parameters of the buck converter prototype are listed in Table I. Control scheme is implemented using a TI TMS320F28377S microcontroller. With reference to Fig. 6, corrected boundary control and voltage ripple measurement algorithms are implemented in interrupt service routine (ISR) running at 250 kHz while error amplifier is implemented in a ISR running at 12 kHz. The measured variables are $i_L$, $i_C$, $v_C$ and $v_S$ and all of them are sampled at 250 kHz. Sampling frequency of 250 kHz is decided based on the maximum switching frequency ($f_S$) of the system which is considered to be 10 kHz for this prototype. The $f_S$ will be depending on buck-stage LC filter parameters, voltage band as well as the type of load since it is inversely proportional to $C_L$ as given in (15). The proposed controller is evaluated with different loads including resistive-capacitive parallel (R//C) loads, a boost converter and a dc electronic load to validate its robustness.

### *A. With R//C Load*

In order to evaluate the dynamic response of the proposed method with linear loads, converter is operated with R//C loads. Fig. 16 compares the steady state waveforms of the buck converter with the proposed $\sigma_{cor}^2$ and $\sigma^2$. Converter is operated with a R//C load of 20Ω and 20μF. It is observed that under $\sigma_{cor}^2$, the output voltage can be regulated within the specified voltage band around a given reference Fig. 17 shows the system performance during a load transient. Here, the load was increased from 25Ω//20μF to 10Ω//20μF with both $\sigma_{cor}^2$ and $\sigma^2$, resulting in the converter reaching its new steady state operating point within 400μs. Noticed that while both controllers have similar transient response times, $\sigma_{cor}^2$ provides a constant voltage ripple size before and after the transient. This validates that the boundary controller performance is unaffected by the bandwidth of the outer feedback loop. Fig. 19 (a) illustrates the converter trajectories on $i_L$-$v_C$ state plane during load

transient. This verifies that the output voltage is maintained within the specified band with $\sigma_{cor}^2$ with a greater accuracy. Also, the state trajectory during the transient closely follows an inherent state-plane trajectory of the equivalent system considering $C_L$ as well. To further evaluate the performance of controller, the reference voltage is changed while converter is connected to a R//C load of 25Ω//20μF. The voltage reference has been changed from 50V to 75V and transient results are presented in Fig. 18.There is an observable overshoot in the voltage waveform with conventional $\sigma^2$, and system performance is degraded significantly in terms of output voltage and current ripple as well as the switching frequency of the system. Fig. 19 (b) show the corresponding performance of the converter with $\sigma_{cor}^2$ in time domain and on $i_L$-$v_C$ state plane. The start-up transient response with $\sigma_{cor}^2$ in time-domain and state-plane are shown by Fig. 20. Results presented reveal that $\sigma_{cor}^2$ provides a significant improvement in comparison with $\sigma^2$ for regulating the output voltage when a R//C connected as a load.

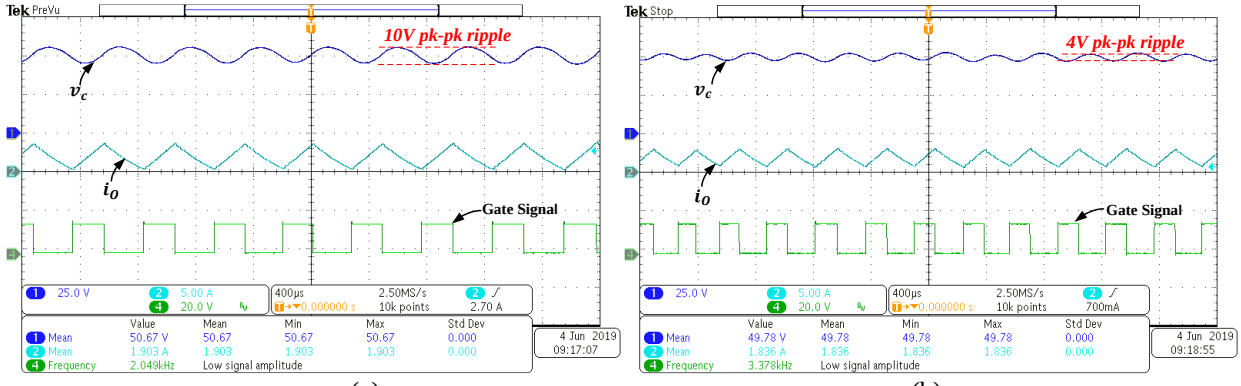


(a) (b)

Fig. 16 Experimental results with a R//C load ($R_L$=25Ω, $C_O$=20μF, Δ =2 V and $v_{ref}$= 50V) (a) with $\sigma^2$ (b) with $\sigma_{cor}^2$.

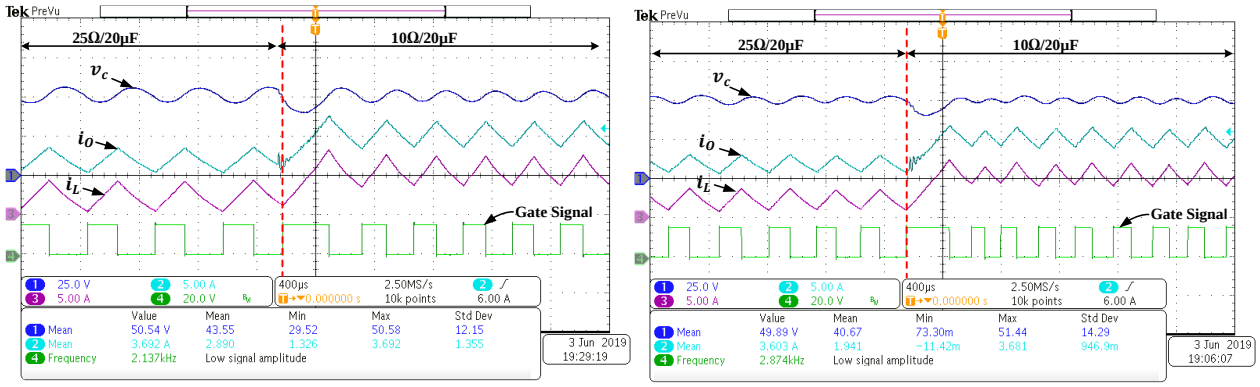


(a) (b)

Fig. 17 Converter transient response when RC load is increased from 25Ω//20μF to 10 Ω//20μF with Δ =2 V and $v_{ref}$= 50V (a) with $\sigma^2$ (b) with $\sigma^2_{cor}$.

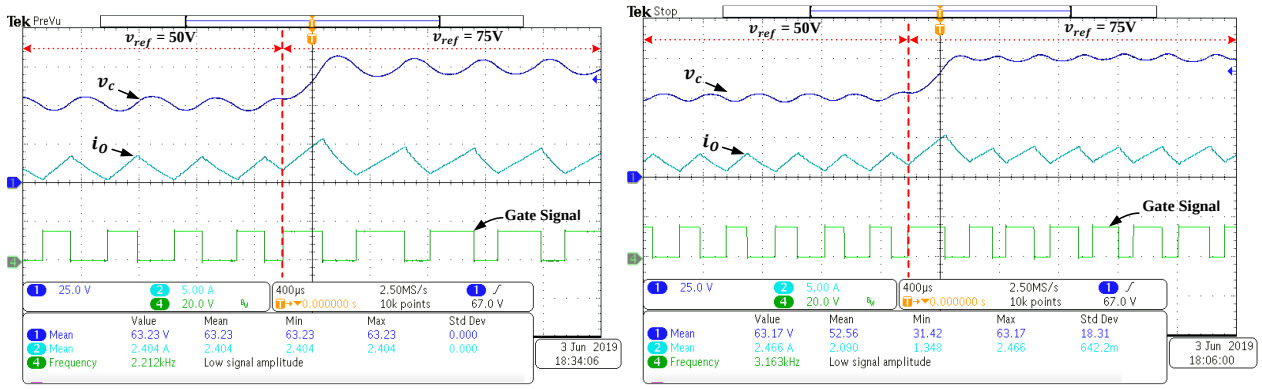


(a) (b)

Fig. 18 Converter transient response for reference voltage from 50V to 75V with a R//C load ($R_L$=25 Ω , $C_L$=20μF, Δ =2 V and $v_{ref}$= 50V) (a) with $\sigma^2$ (b) with $\sigma^2_{cor}$.

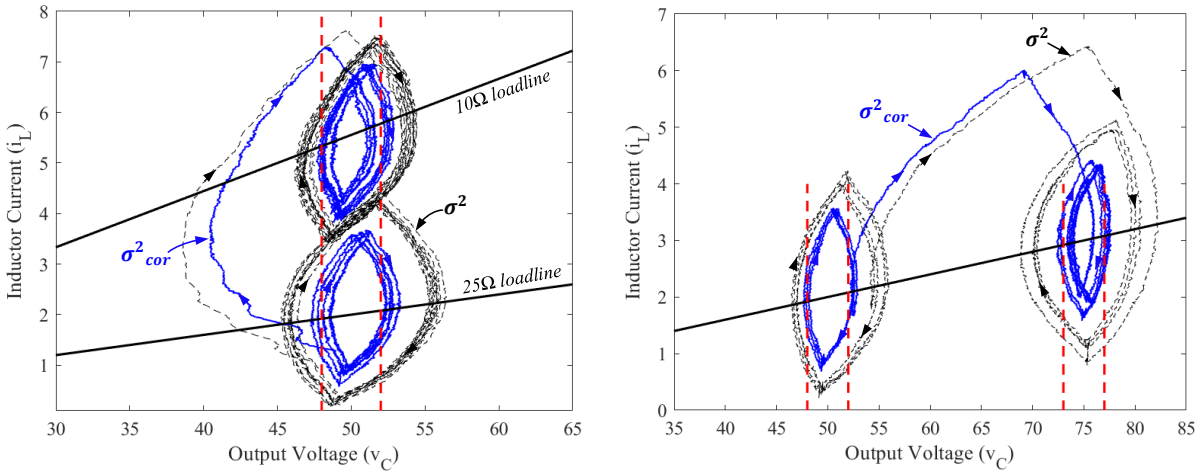


(a) (b)

Fig. 19 State plane trajectory during transients with a R//C load (a) load is increased from 25Ω//20μF to 10 Ω//20μF (b) reference voltage from 50V to 75V.

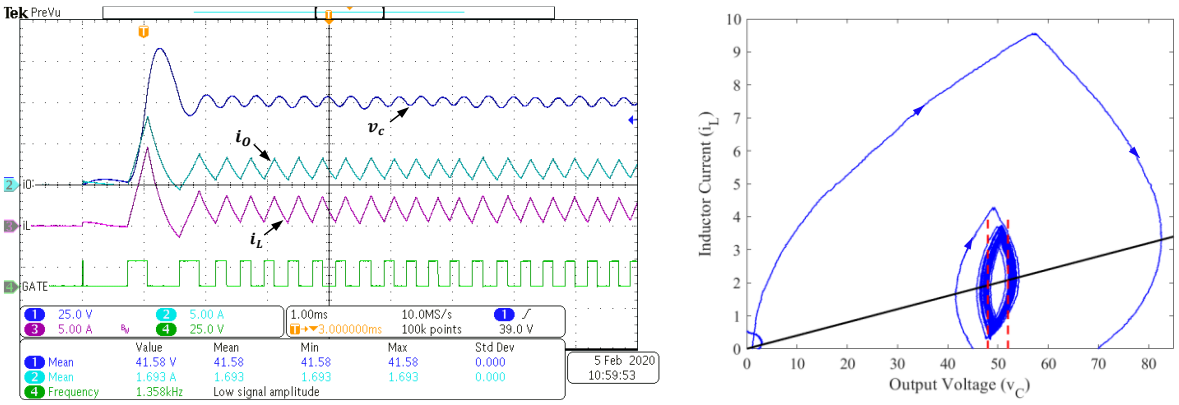


(a) (b)

Fig. 20 Startup transient response results for R//C load of 25Ω//20μF (a) time domain. (b) state-plane.

TABLE IV
PARAMETER VALUES OF BOOST CONVERTER IN EXPERIMENTS

| Parameter | Value | Parameter | Value |
|---|---|---|---|
| $L_B$ | 3.5 mH | $f_{S2}$ | 10 kHz |
| $C_L$ | 100 µF | $R_L$ | 25 Ω |

## *B. Boost Converter as Load*

The steady state operation and transient performance under a reference voltage change of the buck-boost cascaded system are evaluated with proposed control scheme and results are shown in Fig. 21. The boost converter is operated with open loop control and parameters of the boost converter prototype are listed in Table IV. Fig. 21(a) shows the steady state waveforms of both buck and boost converter and it verifies that the output voltage ripple is closely tracked within the specified band. The measured switching frequency is about 1.66 kHz which is close to the theoretical switching frequency of 1.57 kHz under this testing condition. Fig. 21(b) illustrates dynamic response for 50 V – 25 V reference voltage transient. The output voltage approaches the target operating point with two switching actions and recorded transient response time is approximately 1.2 ms. It should be noted that transient response time is limited by input filter dynamics of the boost converter as it is operated with open loop control. Results showed that under proposed $\sigma_{cor}^2$, output voltage can be regulated at specified voltage band. Moreover, the experimental results obtained closely matches with those from simulations.

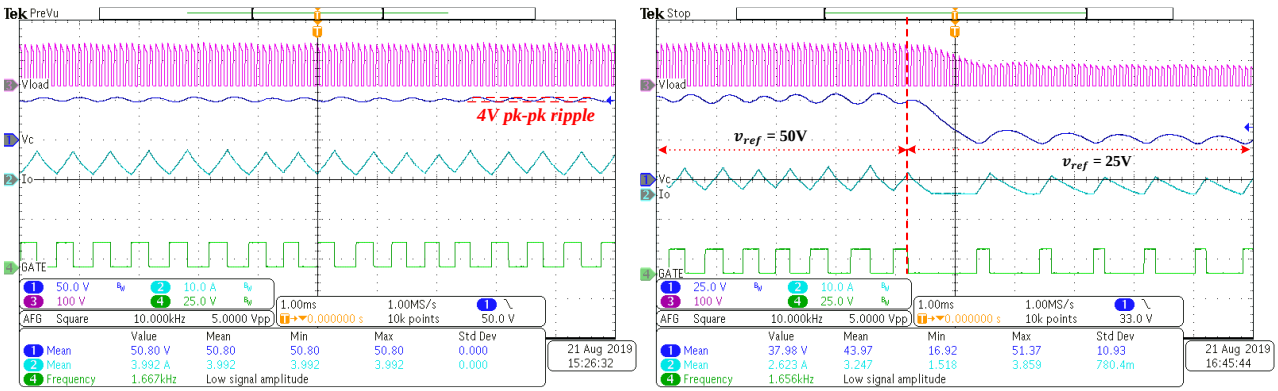


(a) (b)

Fig. 21 Experimental results with the boost converter (a) steady state operation. (b) voltage reference change from 50 V to 25 V. (Δ =2 V, $R$= 25 Ω).

The operating switching frequency of the boost converter is changed from 20 kHz to 5 kHz to validate the proposed control scheme when current ripple of the boost-stage inductor is ~20% of the rated dc current. Fig. 22 shows that $v_C$ is maintained at designed voltage band even when current ripple of boost stage inductor is ~ 30 % of the nominal dc value. This validates that theoretical approximations that considered to derive the control law for cascaded buck-boost systems.

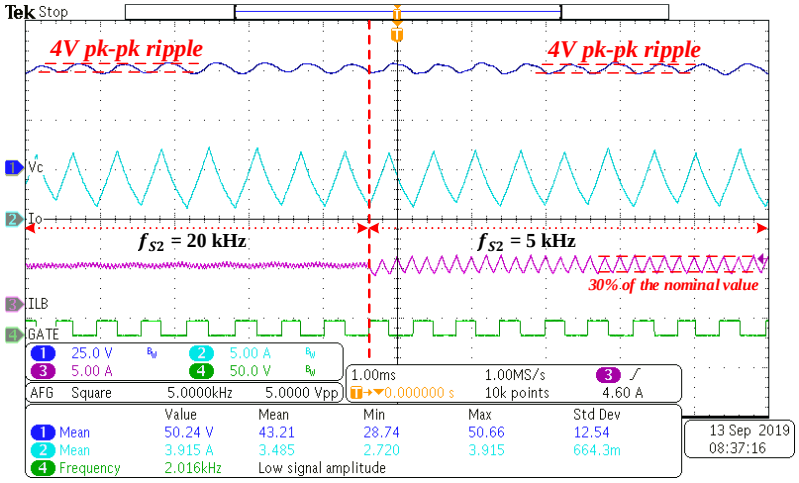


Fig. 22 Experimental results with the boost converter when $f_{S2}$ varied from 20 kHz to 5 kHz ($\Delta$ =2 V, $R$= 25 Ω).

### *C. With DC Electronic Load*

In order validate the proposed method with an unknown non-linear load, buck converter is connected to a commercial DC electronic load (KEIETHLY 2380-500-30). It is operated in constant resistance (CR) form in this test setup. Fig. 23 compares the steady state operation for conventional $\sigma^2$ and proposed $\sigma_{cor}^2$. It is evident that the output voltage is not regulated significantly with $\sigma^2$ due to incorrect switching actions. The voltage ripple is 35 V that is much higher than specified voltage ripple of 4 V and switching frequency is ~2.27 kHz. Contrarily, the output voltage is maintained within the specified band with $\sigma_{cor}^2$ with a greater accuracy. Load step-down and load step-up transients for the proposed method are shown in Fig. 24. As expected, transient response of the buck converter is limited by dynamic response of the DC electronic load. The steady state voltage ripple is

maintained at 4 V at given reference 50 V. The recorded transient response time is approximately ~7 ms for both step-up and step-down transients.

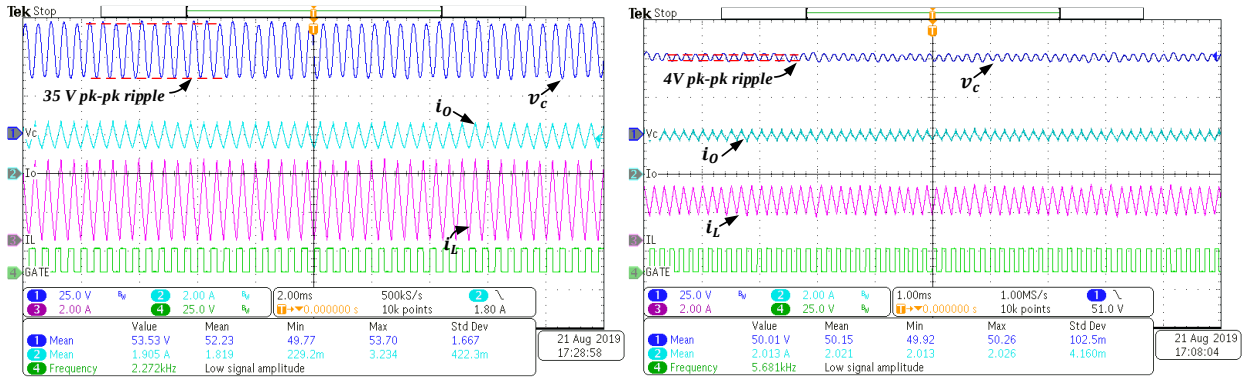


(a) (b)

Fig. 23 Experimental results for steady state operation with DC electronic load ($R_L$=25 Ω , Δ =2 V and $v_{ref}$= 50V) (a) with $\sigma^2$. (b) with $\sigma^2_{cor}$.

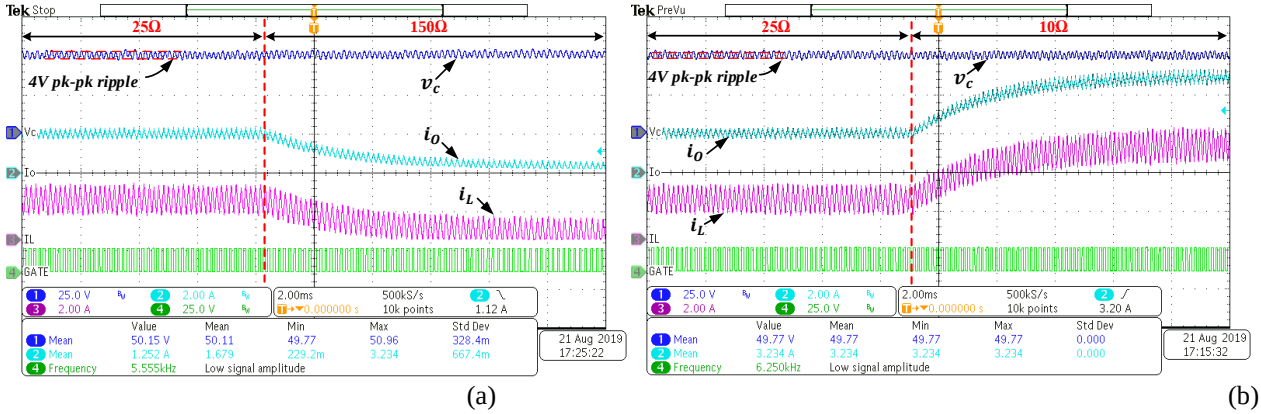


(a) (b)

Fig. 24 Experimental results using $\sigma^2_{cor}$ for load transients through DC electronic load (Δ =2 V and $v_{ref}$= 50V) (a) load step down (25Ω -150Ω). (b) load step up (25Ω -10Ω).

### *D. Challenges in Implementation*

In practical implementation, switching frequency of boundary control will be limited by required computational time and ADC sampling rate. This is because, it requires more computational time to execute instruction codes and its switching actions are dependant on instantaneous measured values [19]. The microcontroller (TMS320F28377S) has 2 ADC channels with a maximum sampling rate of 3.5 MSPS for each channel. Four signals need to be measured for the proposed control architecture, hence actual maximum sampling rate is reduced to 1.75 MSPS. Considering the program

length and execution time, noticed that maximum inner loop operating frequency will be limited to 500 kHz. Hence, target switching frequency will be limited to 10 kHz based on 50 points per cycle. In simulation, there is no upper limit to the system operating frequency and as given in (15), switching frequency can be increased by minimizing filter parameters and voltage band. Simulation results are provided with 30 kHz operating switching frequency to verify the proposed control theory under high switching frequency operation. This validates the theoretical concept of the proposed controller and proves that high switching frequency operation can be achieved by implementing the controller in improved hardware environment.

## VI. CONCLUSIONS

Boundary control techniques that depend on filter parameters and capacitor current needs a corrected switching surface to deal with capacitive and non-linear switching loads. Conventional boundary control with curved switching surface techniques are designed by taking nominal filter parameters and constant load current. Hence, any discrepancies between the switching surface and real system parameters would lead to undesirable output voltage ripple and switching frequency. This paper extends the conventional boundary control with second-order switching surface technique for buck converters cascaded to second-stage boost converters with a capacitive input filter.

The proposed corrected switching surface is applicable for any type of linear load and non-linear switching loads which has a negligible impact on the filter capacitor current from the current ripple components generated due to switching of second-stage converter. The outer feedback loop is implemented to determine the corresponding switching criteria gain factor which accounts for unknown load capacitance or filter parameter deviations, while maintaining the output voltage ripple at a specified voltage band. A simple methodology is introduced to detect the output voltage ripple amplitude using instantaneous measurement of the output voltage and the inductor current.This concept has been validated by both simulations and experimental results under different loads

including boost converter, R//C load and dc electronic load.The results are in good agreement with the theoretical concept and indicate that the proposed corrected boundary control law suppresses the deviation of the switching trajectory in state plane effectively.

## APPENDIX

*A. Derivation of (8) and (10)*

In Turn-ON state , using the Kirchhoff's voltage law,

$$v_{Cmin} - v_C(t_1) = \frac{1}{C}\int_{t_1}^{t_2} i_C \, dt \tag{A.1}$$

between $i_C$ and $t$ in the time interval $t_1$-$t_2$ is derived by assuming it's a straight line,

$$i_C(t) = \frac{di_C(t)}{dt}.\Delta t + i_C(0) \tag{A.2}$$

Voltage across inductor when S is on,

$$v_L = L.\frac{di_L(t)}{dt} = v_S - v_C(t) \tag{A.3}$$

Using (7) and (A.3)

$$(1 + k_D)\frac{di_C(t)}{dt} = \frac{di_L(t)}{dt} = \frac{v_S - v_C(t)}{L} \tag{A.4}$$

Solving (A.2) from $t_1$-$t_2$ , considering at $t_2$,

$i_C(\mathrm{t}_2) = 0$ and then (A.4) yields to,

$$\Delta t = t_1 - t_2 = -\frac{L}{v_S - v_C(t)}[1 + k_D]i_C(t_1) \tag{A.5}$$

The shaded area under $i_C$, $A_1$ can be approximated by a triangle. Thus it can be formulated as,

$$\int_{t_1}^{t_2} i_C \, dt \cong \frac{1}{2} i_C(t_1).\Delta t = -\left[\frac{L}{2(v_S - v_C(t_1))}\right][1 + k_D]{i_C}^2(t_1) \tag{A.6}$$

(8) can be obtained by combining (A.1) and (A.6).

During Turn-OFF state , applying the Kirchhoff's voltage law,

$$v_{Cmax} - v_C(t_3) = \frac{1}{C}\int_{t_3}^{t_4} i_C\, dt \tag{A.7}$$

The shaded area under $i_C$, $A_2$ can be approximated by a triangle.

$$\int_{t_3}^{t_4} i_C\, dt = \left[\frac{L}{2v_C(t_3)}\right][1 + k_D]{i_C}^2(t_3) \tag{A.8}$$

(10) can be obtained by combining (A.7) and (A.8).

*B. Derivation of (15)*

By substituting (4) into inductor voltage equation during Turn-ON state and Turn-OFF state , it can be shown that,

$$t_3 - t_1 = L(1 + k_D)\left[\frac{i_C(t_3) - i_C(t_1)}{v_S - v_{ref}}\right] \tag{B.1}$$

$$t_5 - t_3 = -L(1 + k_D)\left[\frac{i_C(t_5) - i_C(t_3)}{v_{ref}}\right] \tag{B.2}$$

Voltage ripple in steady state for this configuration will be derived as,

$$\Delta = \frac{v_{ref}(1-d)}{16LCf_S^2(1+k_D)} \tag{B.3}$$

Use of (4) and (A.3) into (A.1) for $t_1 \leq t < t_3$

$$v_C(t) = v_{ref} - \Delta + \frac{v_S(1-d)}{2LC(1+k_D)}(t - t_2)^2 \tag{B.4}$$

Also

$$(t_1 - t_2) = (t_2 - t_3) = -\frac{d}{2f_S} \tag{B.5}$$

By substituting (B5) into (B.4)

$$v_C(t_1) = v_C(t_3) = v_{ref} - 2\Delta(d - \tfrac{1}{2}) \tag{B.6}$$

Substituting (B.6) in to (8) and (10),

$$i_C(t_1) = i_C(t_5) = \sqrt{\frac{2\Delta d}{k_1'}} \tag{B.7}$$

$$i_C(t_3) = \sqrt{\frac{2\Delta(1-d)}{k_2'}} \tag{B.8}$$

where $d = \frac{v_{ref}}{v_S}$. Thus, substituting (B.7) and (B.8) into (B.1) and (B.2) will provide (15).

## REFERENCES


[1] W. W. Burns and T. G. Wilson, "A State-Trajectory Control Law for DC-to-DC Converters," *IEEE Trans. Aerosp. Electron. Syst.*, vol. AES-14, no. 1, pp. 2–20, 1978.

[2] M. Greuel, R. Muyshondt, and P. T. Krein, "Design approaches to boundary controllers," in *PESC97. Record 28th Annual IEEE Power Electronics Specialists Conference. Formerly Power Conditioning Specialists Conference 1970-71. Power Processing and Electronic Specialists Conference 1972*, 1997, pp. 672–678.

[3] R. Munzert and P. T. Krein, "Issues in boundary control," *PESC Rec. - IEEE Annu. Power Electron. Spec. Conf.*, vol. 1, pp. 810–816, 1996.

[4] C. Macaulay *et al.*, "United States Patent," vol. 23, no. 10, pp. 1806–1811, 1998.

[5] L. Corradini, E. Orietti, P. Mattavelli, and S. Saggini, "Digital hysteretic voltage-mode control for DC-DC converters based on asynchronous sampling," *IEEE Trans. Power Electron.*, vol. 24, no. 1, pp. 201–211, 2009.

[6] C. N.-M. Ho, V. S. P. Cheung, and H. S.-H. Chung, "Constant-Frequency Hysteresis Current Control of Grid-Connected VSI Without Bandwidth Control," *IEEE Trans. Power Electron.*, vol. 24, no. 11, pp. 2484–2495, 2009.

[7] S. C. Tan, Y. M. Lai, M. K. H. Cheung, and C. K. Tse, "On the practical design of a sliding mode voltage controlled buck converter," *IEEE Trans. Power Electron.*, vol. 20, no. 2, pp. 425–437, 2005.

[8] A. Poveda, E. Fossas, E. Alarcon, F. Guinjoan, and D. Biel, "Application of sliding-mode control to the design of a buck-based sinusoidal generator," *IEEE Trans. Ind. Electron.*, vol. 48, no. 3, pp. 563–571, 2002.

[9] R. Ling, D. Maksimovic, and R. Leyva, "Second-order sliding-mode controlled synchronous buck DC-DC converter," *IEEE Trans. Power Electron.*, vol. 31, no. 3, pp. 2539–2549, 2016.

[10] G. Bartolini, A. Pisano, E. Punta, and E. Usai, "A survey of applications of second-order

sliding mode control to mechanical systems," *Int. J. Control*, vol. 76, no. 9–10, pp. 875–892, 2003.

[11] A. Levant, "Sliding order and sliding accuracy in sliding mode control," *Int. J. Control*, vol. 58, no. 6, pp. 1247–1263, 1993.

[12] K. K. S. Leung and H. S. H. Chung, "Derivation of a second-order switching surface in the boundary control of buck converters," *IEEE Power Electron. Lett.*, vol. 2, no. 2, pp. 63–67, 2004.

[13] K. S. Leung and H. S. H. Chung, "A Comparative Study of the Boundary Control of Buck Converters Using First- and Second-Order Switching Surfaces -Part I: Continuous Conduction Mode," *IEEE 36th Conf. Power Electron. Spec. 2005.*, pp. 2133–2139, 2005.

[14] K. K. S. Leung and H. S. H. Chung, "A comparative study of boundary control with first- and second-order switching surfaces for buck converters operating in DCM," *IEEE Trans. Power Electron.*, vol. 22, no. 4, pp. 1196–1209, 2007.

[15] M. Ordonez, M. T. Iqbal, and J. E. Quaicoe, "Selection of a curved switching surface for buck converters," *IEEE Trans. Power Electron.*, vol. 21, no. 4, pp. 1148–1153, 2006.

[16] J. M. Galvez, M. Ordonez, T. T. Nguyen, and F. Luchino, "Boundary control of buck-boost converters: Normalized trajectories and the Natural Switching Surface," *2012 IEEE Energy Convers. Congr. Expo. ECCE 2012*, pp. 358–363, 2012.

[17] J. M. Galvez and M. Ordonez, "High performance boundary control of boost-derived PFCs: Natural switching surface derivation and properties," *IEEE Trans. Power Electron.*, vol. 27, no. 8, pp. 3807–3816, 2012.

[18] K. K. S. Leung, J. Y. C. Chiu, and H. S. H. Chung, "Boundary Control of Inverters Using Second-Order Switching Surface," *2005 IEEE 36th Power Electron. Spec. Conf.*, vol. 31, pp. 936–942, 2005.

[19] W. T. Yan, C. N. M. Ho, H. S. H. Chung, and K. T. K. Au, "Fixed-frequency boundary control of buck converter with second-order switching surface," *IEEE Trans. Power Electron.*, vol. 24, no. 9, pp. 2193–2201, 2009.

[20] Y. He and H. S. H. Chung, "Use of boundary control with second-order switching surface to reduce the system order for deadbeat controller in grid-connected inverter," *2015 IEEE Energy Convers. Congr. Expo. ECCE 2015*, vol. 31, no. 3, pp. 5129–5136, 2015.

[21] M. Pokharel, N. Hildebrandt, C. N. M. Ho, and Y. He, "A Fast-Dynamic Unipolar Switching Control Scheme for Single-Phase Inverters in DC Microgrids," *IEEE Trans. Power Electron.*, vol. 34, no. 1, pp. 916–927, 2019.

[22] H. S. H. Chung, R.-T. Li, K. K. M. Siu, C. N. M. Ho, and Y. He, "Advanced Digital Controller

for Improving Input Current Quality of Integrated Active Virtual Ground-Bridgeless PFC," *IEEE Trans. Power Electron.*, vol. 34, no. 4, pp. 1–1, 2018.

[23] C. H. M. Ho, H. S. H. Chung, and K. K. S. Leung, "Fast dynamic control of PFC using boundary control with a second-order switching surface," *PESC Rec. - IEEE Annu. Power Electron. Spec. Conf.*, no. 1, pp. 1–7, 2006.

[24] R. Ahmadi, "Dynamic modeling , stability analysis , and controller design for DC distribution systems," *PHD Diss. MISSOURI Univ. Sci. Technol.*, 2013.

[25] A. Riccobono and E. Santi, "Comprehensive review of stability criteria for DC power distribution systems," *IEEE Trans. Ind. Appl.*, vol. 50, no. 5, pp. 3525–3535, 2014.

[26] S. Buck, D. C. Dc, E. Alarcón, L. Pao, S. Member, and D. Maksimovic, "Proximate Time-Optimal Digital Control for Synchronous Buck DC-DC Converters," *IEEE Trans. Power Electron.*, vol. 23, no. 4, pp. 2018–2026, 2018.

[27] A. Babazadeh and D. Maksimović, "Hybrid digital adaptive control for fast transient response in synchronous buck DC-DC converters," *IEEE Trans. Power Electron.*, vol. 24, no. 11, pp. 2625–2638, 2009.

[28] R. Manual, "Switch−Mode Power Supply Reference Manual," 2002.

[29] I. D. G. Jayawardana, C. N. M. Ho, M. Pokharel, and G. Escobar, "A fast dynamic photovoltaic simulator with Instantaneous Output Impedance Matching controller," *2017 IEEE Energy Convers. Congr. Expo. ECCE 2017*, vol. 2017-Janua, pp. 5126–5132, 2017.

[30] A. Koran, K. Sano, R. Y. Kim, and J. S. Lai, "Design of a photovoltaic simulator with a novel reference signal generator and two-stage LC output filter," *IEEE Trans. Power Electron.*, vol. 25, no. 5, pp. 1331–1338, 2010.

[31] F. Gao, B. Blunier, M. G. Simões, and A. Miraoui, "PEM fuel cell stack modeling for real-time emulation in hardware-in-the-loop applications," *IEEE Trans. Energy Convers.*, vol. 26, no. 1, pp. 184–194, 2011.

[32] K. Nguyen-Duy, A. Knott, and M. A. E. Andersen, "High dynamic performance nonlinear source emulator," *IEEE Trans. Power Electron.*, vol. 31, no. 3, pp. 2562–2574, 2016.

[33] R. W. Erickson and D. Maksimovic, *Fundamentals of Power Electronics 2nd Edition*. 2004.

[34] J. Viinamäki, J. Kivimäki, T. Suntio, and L. Hietalahti, "Design of boost-power-stage converter for PV generator interfacing," *2014 16th Eur. Conf. Power Electron. Appl. EPE-ECCE Eur. 2014*, pp. 1–10, 2014.

[35] J. Simonelli, and D. Torrey. "Input Filter Design Considerations for Boost-Derived High Power-Factor Converters." [Proceedings] APEC'92 Seventh Annual Applied Power Electronics Conference and Exposition. IEEE, 1992. 186–192." .